# Fragmentation of positronium with excitation and ionization of the target

C. Starrett,[1] Mary T. McAlinden,[2] and H. R. J. Walters[1]
[1]*Department of Applied Mathematics and Theoretical Physics, Queen's University, Belfast BT7 1NN, United Kingdom*
[2]*School of Computing and Mathematical Sciences, Oxford Brookes University, Wheatley Campus, Oxford OX33 1HX, United Kingdom*
(Received 29 January 2008; published 7 April 2008)

Calculations of positron and electron ejection cross sections are made for collisions of Ps $(1s)$ with the noble gases He, Ne, Ar, Kr, and Xe, allowing for target excitation (i.e., discrete excitation and ionization). Cross sections doubly differential and singly differential with respect to ejected energy and angle are reported, as well as total ionization cross sections. Our results show clearly that excitation of the target becomes very important at impact energies greater than about 2 times the ionization threshold of the atom. Comparison is made with absolute experimental measurements on He and Xe targets and, with one exception, good agreement is found at both total and single differential levels. Unfortunately, most of the measurements are at impact energies where target excitation is small or negligible. There is a need for experiments at higher impact energies to assess the predictions for target excitation.

DOI: 10.1103/PhysRevA.77.042505 PACS number(s): 36.10.Dr

## I. INTRODUCTION

In a previous publication [1] we studied fragmentation of positronium (Ps) in collision with noble-gas targets, but under the assumption that the target was not excited or ionized [so-called "target elastic" (TE) collisions [2]]. The vehicle for this study was the impulse approximation (IA) which treats the scattering of Ps by the target as a coherent combination of free electron and free positron scattering. Comparison was made with absolute experimental data for a He target [3,4] on total Ps fragmentation and on the cross-section differential in the longitudinal (with respect to the direction of the incident Ps beam) energy of the ejected positron. Remarkably good agreement was found with all aspects of the experiments. For comparison with experiment, restriction to TE collisions was appropriate since the impact energies were sufficiently low ($\leq 33$ eV) that either the He target could not be excited or ionized ($\leq 27$ eV) or, if it could, such processes would be negligible. With increasing impact energy we are faced with having to take account of inelastic processes in the target. Whether these be discrete excitations or ionization of the target we shall, for convenience, henceforth refer to them simply as target "excitation." It is the purpose of this article to address this issue.

In dealing with target excitation we need to sum over all final states of the target atom that can be accessed at a particular impact energy. This in itself is a difficult enough problem. In order to have a feasible approach, we have therefore elected to calculate target excitation collisions in the first Born approximation (FBA), employing ideas of Hartley and Walters [5] for performing the sum over excited states. The use of the FBA for target inelastic (TI) collisions contrasts with the use of the IA for TE collisions and so some words need to be said about this.

In the FBA the amplitude for a collision in which the Ps goes from state $\phi_a$ to $\phi_{a'}$ while the atom changes from state $\psi_b$ to $\psi_{b'}$ is given by [1,6]

$$f^{B1}(\mathrm{Ps}{:}a \to a';\mathrm{atom}{:}b \to b') = -\frac{4}{q^2} I^{\mathrm{Ps}}_{aa'}(\boldsymbol{q}) I^{\mathrm{at}}_{bb'}(\boldsymbol{q}), \quad (1)$$

where

$$I^{\mathrm{Ps}}_{aa'}(\boldsymbol{q}) \equiv \langle \phi_{a'}(\boldsymbol{t}) | e^{-i\boldsymbol{q}\cdot\boldsymbol{t}/2} - e^{i\boldsymbol{q}\cdot\boldsymbol{t}/2} | \phi_a(\boldsymbol{t}) \rangle, \quad (2a)$$

$$I^{\mathrm{at}}_{bb'}(\boldsymbol{q}) \equiv \langle \psi_{b'}(\boldsymbol{X}) | (Z - \sum_{i=1}^{Z} e^{i\boldsymbol{q}\cdot\boldsymbol{r}_i}) | \psi_b(\boldsymbol{X}) \rangle. \quad (2b)$$

In (1), (2a), and (2b), $\boldsymbol{q}=\boldsymbol{p}_0-\boldsymbol{p}_f$ is the momentum transfer in the collision, $\boldsymbol{p}_0(\boldsymbol{p}_f)$ is the initial (final) momentum of the Ps, $\boldsymbol{t}$ is the Ps internal coordinate, $\boldsymbol{X}$ stands for the space and spin coordinates of the atomic electrons, $\boldsymbol{r}_i$ is the space coordinate of the $i$th atomic electron, and it is assumed that the target is a neutral atom containing $Z$ electrons. It is noteworthy that the amplitude (1) is the product of two form factors $I^{\mathrm{Ps}}_{aa'}$ and $I^{\mathrm{at}}_{bb'}$, which refer separately to the transitions in the Ps and the atom, respectively.

When the final state of the atom is the same as the initial state, $\psi_{b'}=\psi_b$ (a TE process), the matrix element (2b) scales with $Z$ with the result that the magnitude of the FBA amplitude grows as the target atom increases in size. This eventually results in a violation of unitarity, giving cross sections that are too large. This point has been well documented [2,7–10]. Since we wish to treat targets of any size we must therefore seek a nonperturbative approximation for TE collisions. The IA provides a good practical solution.

By contrast, when the atom is excited, $\psi_{b'} \neq \psi_b$ (a TI process), the nuclear charge $Z$ disappears from (2a) and (2b) by orthogonality. Further, in an independent-particle model of the atom in which the wave functions are represented by single Slater determinants composed out of orthonormal spin orbitals $\chi_i$, Eq. (2b) reduces to

$$I^{\mathrm{at}}_{bb'} = -\langle \chi_{b'} | e^{i\boldsymbol{q}\cdot\boldsymbol{r}} | \chi_b \rangle, \quad (3)$$

where we assume that the states $\psi_b$ and $\psi_{b'}$ differ only by the spin orbitals $\chi_b$ and $\chi_{b'}$; if they differ by more than one spin orbital, then $I^{\mathrm{at}}_{bb'}=0$. The result (3) tells us that, in the FBA, excitation of the atom is very much a one-electron process. We therefore expect the FBA for an inelastic transition in the atom to remain reasonable irrespective of the size of the atom, unlike TE scattering. Experience [8–11] bears this out.

 

This is not to say that the FBA is perfect, but rather that it gives a reasonable estimate of the inelastic events. The important practical point, however, is that the FBA provides a feasible route for summing over all final excited states of the target.

In studying fragmentation of Ps we may choose either to measure the positrons that come off or the electrons. It was shown in [1] that for TE collisions differential cross sections for positron and electron ejection are, in general, different; although asymptotically in impact energy, when the FBA is valid, they become identical. A weakness in using the FBA to describe TI fragmentation is that this distinction between the ejected positron and electron is lost. While detection of a positron is a definite signal that the Ps has fragmented, a detected electron may have come either from fragmentation of the Ps or from ionization of the atom, if both fragment we get two counts in our detector (assuming that the atom is only singly ionized, multiple ionization of the atom is much less likely). In looking at electron detection we must therefore take account of electrons ionized from the target. We also address this problem here.

The structure of this paper is as follows. In Sec. II we introduce the cross sections of interest: double-differential (DDCS), single-differential (SDCS), and total ionization cross sections, for both electron and positron ejection. Section III A develops a model of TI collisions based on the FBA using the approximation of Hartley and Walters [5] to sum over all final atom states. In Sec. III B the FBA is used again to model electrons ejected from the target atom while the final state of the Ps remains unobserved [a (TT) process]. Section IV reviews necessary calculational details while in Sec. V results are presented. In Sec. V A we look at total ionization cross sections for the noble gases He, Ne, Ar, Kr, and Xe, with experimental comparisons for He and Xe. Section V B describes our SDCS results, where now and henceforth we limit ourselves to the extreme cases of He and Xe. Here experimental comparison is made for He. Last, the DDCSs are presented in Sec. V C, where a select sample of results is used to give a flavor of these cross sections. Finally, conclusions are drawn in Sec. VI.

## II. CROSS SECTIONS

From (1) and formula (22) of [1], the triple-differential cross section (TDCS) for fragmentation of the Ps in the FBA is given by

$$\frac{d^3\sigma^{B1}_{bb'}}{dE\, d\Omega_e\, d\Omega_p} = \frac{4v_p v_e}{v_0}\frac{1}{q^4}|I^{\mathrm{Ps}}_{a\boldsymbol{\kappa}}(\boldsymbol{q})|^2|I^{\mathrm{at}}_{bb'}(\boldsymbol{q})|^2, \tag{4}$$

where we consider a specific transition $\psi_b \to \psi_{b'}$ in the atom, $\boldsymbol{v}_p$ ($\boldsymbol{v}_e$) is the velocity of the positron (electron) emitted into a solid angle $d\Omega_p(d\Omega_e)$, $\boldsymbol{v}_0$ is the velocity of the incident Ps,

$$\boldsymbol{\kappa} = \frac{1}{2}(\boldsymbol{v}_p - \boldsymbol{v}_e) \tag{5}$$

is the momentum of the positron relative to the electron, and [see (2a)]

$$I^{\mathrm{Ps}}_{a\boldsymbol{\kappa}}(\boldsymbol{q}) = \langle \phi^-_{\boldsymbol{\kappa}}(t)|e^{-i\boldsymbol{q}\cdot\boldsymbol{t}/2} - e^{i\boldsymbol{q}\cdot\boldsymbol{t}/2}|\phi_a(t)\rangle. \tag{6}$$

In (6), $\phi^-_{\boldsymbol{\kappa}}$ is a continuum state of the Ps with relative momentum $\boldsymbol{\kappa}$ and ingoing scattered waves, normalized to

$$\langle \phi_{\boldsymbol{\kappa}}|\phi_{\boldsymbol{\kappa}'}\rangle = \delta(\boldsymbol{\kappa} - \boldsymbol{\kappa}'). \tag{7}$$

Conservation of energy requires that

$$v_0^2 + \epsilon_b = \frac{1}{2}v_p^2 + \frac{1}{2}v_e^2 + \epsilon_{b'} + Q_a^{\mathrm{Ps}} \tag{8a}$$

$$= \kappa^2 + v_f^2 + \epsilon_{b'} + Q_a^{\mathrm{Ps}}, \tag{8b}$$

where $\epsilon_b$ is the energy of the atomic state $\psi_b$, $Q_a^{\mathrm{Ps}}$ is the ionization potential of the Ps state $\phi_a$, and

$$\boldsymbol{v}_f \equiv \frac{1}{2}(\boldsymbol{v}_p + \boldsymbol{v}_e) \tag{9}$$

is the velocity of the center of mass of the fragmented Ps.

The DDCS for positron ejection, $d^2\sigma^{B1}_{bb'}/dE_p d\Omega_p$ [12], is the integral of (4) over all directions of the ejected Ps electron. In [1] it is shown that, in the FBA, electron and positron ejection are identical—i.e.,

$$\frac{d^2\sigma^{B1}_{bb'}}{dE_p d\Omega_p}(\boldsymbol{v}_p = \boldsymbol{v}) = \frac{d^2\sigma^{B1}_{bb'}}{dE_e d\Omega_e}(\boldsymbol{v}_e = \boldsymbol{v}). \tag{10}$$

The (complete) TI contribution to the DDCS for positron or electron ejection is

$$\frac{d^2\sigma^{B1}_{\mathrm{TI}}}{dE_p d\Omega_p} = \sum_{b'\neq b}\frac{d^2\sigma^{B1}_{bb'}}{dE_p d\Omega_p} = \frac{d^2\sigma^{B1}_{\mathrm{TI}}}{dE_e d\Omega_e}, \tag{11}$$

where the sum is over all atom states that can be excited at the given impact energy [see (8a) and (8b)].

Thus the (complete) cross section for positron ejection is the sum of two parts: a TE contribution considered in [1] and a TI contribution (11); we label this sum TOTPOS. Hence, the DDCS for positron ejection is

$$\frac{d^2\sigma^{\mathrm{TOTPOS}}}{dE_p d\Omega_p} = \frac{d^2\sigma^{\mathrm{IA}}_{\mathrm{TE}}}{dE_p d\Omega_p} + \frac{d^2\sigma^{B1}_{\mathrm{TI}}}{dE_p d\Omega_p}. \tag{12}$$

Integration of (12) over all positron ejection angles gives the SDCS

$$\frac{d\sigma^{\mathrm{TOTPOS}}}{dE_p} = \frac{d\sigma^{\mathrm{IA}}_{\mathrm{TE}}}{dE_p} + \frac{d\sigma^{B1}_{\mathrm{TI}}}{dE_p}. \tag{13}$$

Or integration of (12) over positron ejection energies gives the SDCS

$$\frac{d\sigma^{\mathrm{TOTPOS}}}{d\Omega_p} = \frac{d\sigma^{\mathrm{IA}}_{\mathrm{TE}}}{d\Omega_p} + \frac{d\sigma^{B1}_{\mathrm{TI}}}{d\Omega_p}. \tag{14}$$

The total cross section for positron ejection, or equivalently for Ps fragmentation, is then obtained by further integration of (13) or (14):

$$\sigma^{\mathrm{TOTPOS}} = \sigma^{\mathrm{IA}}_{\mathrm{TE}} + \sigma^{B1}_{\mathrm{TI}}. \tag{15}$$

The cross section for electron ejection is the sum of three parts: a TE contribution which was considered in [1]; the TI contribution (11) corresponding to the case where the ejected electron comes from fragmentation of the Ps; and a target (TT) contribution where the ejected electron comes from ionization of the target atom and the final state of the Ps, whether discrete or ionized, remains unobserved. We label this sum TOTELE. The DDCS for electron ejection is thus

$$\frac{d^2\sigma^{\mathrm{TOTELE}}}{dE_e d\Omega_e} = \frac{d^2\sigma^{\mathrm{IA}}_{\mathrm{TE}}}{dE_e d\Omega_e} + \frac{d^2\sigma^{B1}_{\mathrm{TI}}}{dE_e d\Omega_e} + \frac{d^2\sigma^{B1}_{\mathrm{TT}}}{dE_e d\Omega_e}, \tag{16}$$

where

$$\frac{d^2\sigma^{B1}_{\mathrm{TT}}}{dE_e d\Omega_e} = \sum_{a'} \frac{d^2\sigma^{B1}_{aa'}}{dE_e d\Omega_e} \tag{17}$$

and the sum in (17) is over all final Ps states $\phi_{a'}$. The SDCSs are

$$\frac{d\sigma^{\mathrm{TOTELE}}}{dE_e} = \frac{d\sigma^{\mathrm{IA}}_{\mathrm{TE}}}{dE_e} + \frac{d\sigma^{B1}_{\mathrm{TI}}}{dE_e} + \frac{d\sigma^{B1}_{\mathrm{TT}}}{dE_e} \tag{18}$$

and

$$\frac{d\sigma^{\mathrm{TOTELE}}}{d\Omega_e} = \frac{d\sigma^{\mathrm{IA}}_{\mathrm{TE}}}{d\Omega_e} + \frac{d\sigma^{B1}_{\mathrm{TI}}}{d\Omega_e} + \frac{d\sigma^{B1}_{\mathrm{TT}}}{d\Omega_e}, \tag{19}$$

and the total cross section for observing an electron is

$$\sigma^{\mathrm{TOTELE}} = \sigma^{\mathrm{IA}}_{\mathrm{TE}} + \sigma^{B1}_{\mathrm{TI}} + \sigma^{B1}_{\mathrm{TT}}. \tag{20}$$

While there is hope of a DDCS measurement in the near future [13], existing experimental data on fragmentation [3,4,14,15] are only available for single-differential cross sections and the total cross sections (15) and (20). The measured SDCSs are with respect to the longitudinal energy of the ejected positron ($E_{pl}$) (see [1]):

$$\frac{d\sigma^{\mathrm{TOTPOS}}}{dE_{pl}} = \frac{d\sigma^{\mathrm{IA}}_{\mathrm{TE}}}{dE_{pl}} + \frac{d\sigma^{B1}_{\mathrm{TI}}}{dE_{pl}}. \tag{21}$$

It is hoped to have measurements with respect to the longitudinal energy ($E_{el}$) of ejected electrons soon [13]—i.e.

$$\frac{d\sigma^{\mathrm{TOTELE}}}{dE_{el}} = \frac{d\sigma^{\mathrm{IA}}_{\mathrm{TE}}}{dE_{el}} + \frac{d\sigma^{B1}_{\mathrm{TI}}}{dE_{el}} + \frac{d\sigma^{B1}_{\mathrm{TT}}}{dE_{el}}. \tag{22}$$

## III. THEORY

### A. TI collisions

To evaluate (11) we follow the scheme of Hartley and Walters [5]. We restrict ourselves to noble-gas targets and take the initial state $\psi_b$ to be the ground state which we represent by a single Slater determinant composed out of orthonormal spin orbitals $\chi_{nlm}(\boldsymbol{r})\zeta_{s_z}(s)$ [16]. We first assume that all excitations of the target are single-electron ionizations, the ionized states being created by removing a spin orbital $\chi_{nlm}(\boldsymbol{r})\zeta_{s_z}(s)$ from the ground state $\psi_b$ and replacing it by a continuum spin orbital $\chi^-_{nl\boldsymbol{v}_T}(\boldsymbol{r})\zeta_{s_z}(s)$ with the same spin function $\zeta_{s_z}(s)$. We require $\chi^-_{nl\boldsymbol{v}_T}(\boldsymbol{r})$ to be orthogonal to all the orbitals in $\psi_b$ and to be normalized as

$$\langle \chi^-_{nl\boldsymbol{v}_T} | \chi^-_{nl\boldsymbol{v}'_T} \rangle = \delta(\boldsymbol{v}_T - \boldsymbol{v}'_T). \tag{23}$$

We assume that the ionized electron moves in a spherically averaged potential $V_{nl}(r)$ which we take to be the static potential $V_{\mathrm{static}}(r)$ of $\psi_b$ less the spherically averaged contribution from the removed spin orbital $\chi_{nlm}(\boldsymbol{r})\zeta_{s_z}$. Writing

$$\chi_{nlm}(\boldsymbol{r}) = \frac{\chi_{nl}(r)}{r} Y_{lm}(\hat{\boldsymbol{r}}), \tag{24}$$

where $Y_{lm}$ is a spherical harmonic as defined by Rose [18],

$$V_{\mathrm{static}}(r) = 2\sum_{n'l'} (2l'+1) \int_0^\infty \chi_{n'l'}(r') \left( -\frac{1}{r} + \frac{1}{r_>} \right) \chi_{n'l'}(r') dr', \tag{25}$$

where the sum is over all the shells of $\psi_b$ and $r_> = \max(r, r')$. The potential $V_{nl}(r)$ is then given by

$$V_{nl}(r) = V_{\mathrm{static}}(r) - \int \chi_{nl}(r') \frac{1}{r_>} \chi_{nl}(r') dr'. \tag{26}$$

Expanding $\chi^-_{nl\boldsymbol{v}_T}$ in partial waves according to

$$\chi^-_{nl\boldsymbol{v}_T}(\boldsymbol{r}) = \frac{1}{(2\pi)^{3/2}} \sum_{\lambda=0}^{\infty} i^\lambda (2\lambda+1) e^{-i\eta^C_\lambda} \frac{u_{nl\lambda}(v_T, r)}{v_T r} P_\lambda(\hat{\boldsymbol{v}}_T \cdot \hat{\boldsymbol{r}}), \tag{27}$$

where

$$\eta^C_\lambda = \arg \Gamma\left( \lambda + 1 - \frac{i}{v_T} \right) \tag{28}$$

is the Coulomb phase shift and $P_\lambda$ is the Legendre polynomial of order $\lambda$, we require $u_{nl\lambda}$ to satisfy the partial wave Schrödinger equation

$$\left( \frac{d^2}{dr^2} - \frac{\lambda(\lambda+1)}{r^2} - 2V_{nl}(r) + v_T^2 \right) u_{nl\lambda}(v_T, r) = \sum_{n'} \alpha_{n'\lambda} \chi_{n'\lambda}(r), \tag{29}$$

where the $\alpha_{n'\lambda}$ are Lagrange multipliers that make $u_{nl\lambda}$ orthogonal to all the orbitals in $\psi_b$ with angular momentum $\lambda$ [17]. We must choose $\chi^-_{nl\boldsymbol{v}_T}$ to have ingoing scattered wave boundary conditions, so we require that

$$u_{nl\lambda}(v_T, r) \overset{r\to\infty}{\to} \sin\theta_\lambda + f_{nl\lambda} e^{-i\theta_\lambda}, \tag{30}$$

where

$$\theta_\lambda \equiv v_T r - \frac{1}{2}\lambda\pi + \frac{1}{v_T} \ln 2v_T r + \eta^C_\lambda \tag{31}$$

and $f_{nl\lambda}$ is a constant. With this choice $\chi^-_{nl\boldsymbol{v}_T}$ satisfies the normalization condition (23). The Lagrange orthogonalization to all the orbitals of $\psi_b$ is a reasonable approximation to electron exchange effects between the ionized electron and its parent ion [17].

In this picture of atom excitation

$$I^{\mathrm{at}}_{bb'}(\mathbf{q}) \to I^{\mathrm{at}}_{nlm}(\boldsymbol{v}_T,\boldsymbol{q}), \tag{32}$$

where, from (3),

$$I^{\mathrm{at}}_{nlm}(\boldsymbol{v}_T,\boldsymbol{q}) \equiv -\langle \chi^{-}_{nl\boldsymbol{v}_T}(\boldsymbol{r})|e^{i\boldsymbol{q}\cdot\boldsymbol{r}}|\chi_{nlm}(\boldsymbol{r})\rangle. \tag{33}$$

The sum over excited atom states required in (11) then becomes an integral over the energetically allowed values of $\boldsymbol{v}_T$ and a sum over the spin orbitals in $\psi_b$ from which the target electron can be ionized. Using (4), (11), and (32), we therefore write

$$\frac{d^2\sigma^{B1}_{\mathrm{TI}}}{dE_p d\Omega_p} = \sum_{nl} \frac{d^2\sigma^{B1}_{nl}}{dE_p d\Omega_p}, \tag{34a}$$

$$\frac{d^2\sigma^{B1}_{nl}}{dE_p d\Omega_p} = \frac{8v_p}{v_0}\int_0^{v_{T_{\max}}} dv_T v_T^2 \int d\hat{\boldsymbol{v}}_e \frac{v_e}{q^4}|I^{\mathrm{Ps}}_{a\boldsymbol{\kappa}}(\boldsymbol{q})|^2 G^{\mathrm{at}}_{nl}(v_T,q), \tag{34b}$$

where a caret denotes a unit vector,

$$G^{\mathrm{at}}_{nl}(v_T,q) \equiv \int d\hat{\boldsymbol{v}}_T \sum_{m=-l}^{+l} |I^{\mathrm{at}}_{nlm}(\boldsymbol{v}_T,\boldsymbol{q})|^2, \tag{35}$$

and the upper limit on the integration over $v_T$ is determined by the conservation of energy condition [see (8a)]

$$v_0^2 = \frac{1}{2}v_p^2 + \frac{1}{2}v_e^2 + \frac{1}{2}v_T^2 + Q^{\mathrm{Ps}}_a + Q^{\mathrm{at}}_{nl}; \tag{36}$$

i.e.,

$$v_{T_{\max}} = \sqrt{2v_0^2 - 2Q^{\mathrm{Ps}}_a - 2Q^{\mathrm{at}}_{nl} - v_p^2}, \tag{37}$$

$Q^{\mathrm{at}}_{nl}$ being the ionization potential of the atomic $nl$ shell. In (34a) and (34b), $v_e$ is a function of $v_T$ defined by (36), and $\boldsymbol{q}$ and $\boldsymbol{\kappa}$ are functions of $v_T$ and $\hat{\boldsymbol{v}}_e$ defined by

$$\boldsymbol{q} = 2\boldsymbol{v}_0 - \boldsymbol{v}_e - \boldsymbol{v}_p \tag{38}$$

and (5). From (24) and (27), it can be shown that

$$I^{\mathrm{at}}_{nlm}(\boldsymbol{v}_T,\boldsymbol{q}) = \sum_{\lambda=0}^{\infty}\sum_{l'=|\lambda-l|}^{|\lambda+l|} A(\lambda,l',l)R(\lambda,l',l,v_T,q,n) \times \sum_{m'} C(\lambda,l',l,m',m-m',m) \times Y_{\lambda m'}(\hat{\boldsymbol{v}}_T)Y_{l'(m-m')}(\hat{\boldsymbol{q}}), \tag{39}$$

where

$$A(\lambda,l',l) \equiv (-1)^{\lambda+1} i^{\lambda+l'} 2^{3/2}\left[\frac{(2\lambda+1)(2l'+1)}{(2l+1)}\right]^{1/2} \times C(\lambda,l',l,0,0,0), \tag{40}$$

$$R(\lambda,l',l,v_T,q,n) \equiv \frac{e^{i\eta^C_\lambda}}{v_T}\int_0^\infty u_{nl\lambda}(v_T,r) j_{l'}(qr)\chi_{nl}(r)dr, \tag{41}$$

$C(j_1,j_2,j_3,m_1,m_2,m_3)$ is a Clebsch-Gordan coefficient as defined by Rose [18], and $j_l(x)$ is a spherical Bessel function as defined by Abramowitz and Stegun [19]. From (35) and (39) it follows that

$$G^{\mathrm{at}}_{nl}(v_T,q) = \frac{(2l+1)}{4\pi}\sum_{\lambda=0}^{\infty}\sum_{l'=|\lambda-l|}^{|\lambda+l|} |A(\lambda,l',l)|^2 |R(\lambda,l',l,v_T,q,n)|^2, \tag{42}$$

which shows explicitly that $G^{\mathrm{at}}_{nl}(v_T,q)$ depends only upon the magnitudes on $\boldsymbol{v}_T$ and $\boldsymbol{q}$ and not on their directions, as indicated by the notation. The other matrix element $I^{\mathrm{Ps}}_{a\boldsymbol{\kappa}}$ required in (34a) and (34b) may be obtained analytically using the Nordsieck integration technique [20,21].

Following Hartley and Walters [5] we now correct (34a) and (34b) to allow for the existence of excitations other than single ionization (principally discrete excitations) and to compensate for any weaknesses in our approximations to $\psi_b$ and the singly ionized states. This is done by introducing a factor $S(q)/\bar{S}(q)$ where $S(q)$ is the incoherent scattering function

$$S(q) = \sum_{b'\neq b} |\langle \psi_{b'}(\mathbf{X})|Z - \sum_{j=1}^{Z} e^{i\boldsymbol{q}\cdot\boldsymbol{r}_j}|\psi_b(\boldsymbol{X})\rangle|^2 \tag{43a}$$

$$= \langle \psi_b(\boldsymbol{X})|\sum_{j=1}^{Z}\sum_{k=1}^{Z} e^{i\boldsymbol{q}\cdot(\boldsymbol{r}_j-\boldsymbol{r}_k)}|\psi_b(\boldsymbol{X})\rangle - |\langle \psi_b(\boldsymbol{X})|\sum_{j=1}^{Z} e^{i\boldsymbol{q}\cdot\boldsymbol{r}_j}|\psi_b(\boldsymbol{X})\rangle|^2 \tag{43b}$$

and $\bar{S}(q)$ is its analog in our approximation that all excitations are single ionizations. From (2b), (32), (35), (43a), and (43b),

$$\bar{S}(q) = 2\sum_{nl}\int_0^\infty dv_T v_T^2 G^{\mathrm{at}}_{nl}(v_T,q). \tag{44}$$

The factor of 2 in (44) arises from the double-spin occupancy associated with each spatial orbital $\chi_{nlm}(\boldsymbol{r})$. From (43b) it is clear that $S(q)$ is determined entirely by the atomic state $\psi_b$, tabulations are available in the literature (see Sec. IV). Including the factor $S(q)/\bar{S}(q)$, Eq. (34a) and (34b) finally becomes

$$\frac{d^2\sigma^{B1}_{\mathrm{TI}}}{dE_p d\Omega_p} = \sum_{nl}\frac{d^2\sigma^{B1}_{nl}}{dE_p d\Omega_p}, \tag{45a}$$

$$\frac{d^2\sigma_{nl}^{B1}}{dE_p d\Omega_p} = \frac{8v_p}{v_0}\int_0^{v_{T_{\max}}} dv_T v_T^2 \int d\hat{\boldsymbol{v}}_e \frac{v_e}{q^4}|I_{a\boldsymbol{\kappa}}^{\mathrm{Ps}}(\boldsymbol{q})|^2 G_{nl}^{\mathrm{at}}(v_T,q)\frac{S(q)}{\bar{S}(q)}. \tag{45b}$$

As Hartley and Walters [5] point out, the introduction of the $S/\bar{S}$ factor ensures that $d^2\sigma_{\mathrm{TI}}^{B1}/dE_p d\Omega_p$ is correct in the high-impact-energy asymptotic limit. The approximation (45a) and (45b) is appropriate when excitation of the atom is dominated by single-electron ionization. This is expected to be the case for the noble-gas targets studied here [5].

In the FBA the TI contribution to the longitudinal cross section $d\sigma/dE_{pl}$ is given by (see [1])

$$\frac{d\sigma_{\mathrm{TI}}^{B1}}{dE_{pl}} = \sum_{nl}\sum_{\epsilon=-1}^{+1}\frac{\pi}{\sqrt{E_{pl}}}\int_{E_{pl}}^{\bar{E}_{nl}}\frac{d^2\sigma_{nl}^{B1}}{dE_p d\Omega_p} \times\left(E_0,E_p,\cos\theta_p=\epsilon\sqrt{\frac{E_{pl}}{E_p}}\right)\frac{dE_p}{\sqrt{E_p}}, \tag{46}$$

where

$$\bar{E}_{nl} = v_0^2 - Q_a^{\mathrm{Ps}} - Q_{nl}^{\mathrm{at}} \tag{47}$$

and $\epsilon$ takes on the values $-1$ and $+1$. In (46) it is assumed that the DDCS depends only upon the incident Ps energy $E_0=v_0^2$, the ejected positron energy $E_p=\frac{1}{2}v_p^2$, and the angle $\theta_p$ which the positron makes with the incident direction. This is true for the cases studied here where the Ps is in the $1s$ state and the target is a ground-state noble-gas atom. The sum over $\epsilon$ is explained by the fact that experiment collects positrons moving in both the forward ($\cos\theta_p>0$) and backward ($\cos\theta_p<0$) directions (see [1]). Again, we note the equivalence of ejected electron and positron spectra in the FBA (i.e., see [1]):

$$\frac{d^2\sigma_{\mathrm{TI}}^{B1}}{dE_e d\Omega_e}(\boldsymbol{v}_e=\boldsymbol{v}) = \frac{d^2\sigma_{\mathrm{TI}}^{B1}}{dE_p d\Omega_p}(\boldsymbol{v}_p=\boldsymbol{v}), \tag{48a}$$

$$\frac{d\sigma_{\mathrm{TI}}^{B1}}{dE_{el}}(E_{el}=E_l) = \frac{d\sigma_{\mathrm{TI}}^{B1}}{dE_{pl}}(E_{pl}=E_l), \tag{48b}$$

$$\frac{d\sigma_{\mathrm{TI}}^{B1}}{dE_e}(E_e=E) = \frac{d\sigma_{\mathrm{TI}}^{B1}}{dE_p}(E_p=E), \tag{48c}$$

$$\frac{d\sigma_{\mathrm{TI}}^{B1}}{d\Omega_e}(\hat{\boldsymbol{v}}_e=\hat{\boldsymbol{v}}) = \frac{d\sigma_{\mathrm{TI}}^{B1}}{d\Omega_p}(\hat{\boldsymbol{v}}_p=\hat{\boldsymbol{v}}). \tag{48d}$$

To calculate the TI contribution to the total Ps fragmentation cross section $\sigma_{\mathrm{TI}}^{B1}$, it is more convenient to start from

$$\frac{d^3\sigma_{bb'}^{B1}}{d\hat{\boldsymbol{v}}_f d\boldsymbol{\kappa}} = \frac{16v_f}{v_0}\frac{1}{q^4}|I_{a\boldsymbol{\kappa}}^{\mathrm{Ps}}(\boldsymbol{q})|^2|I_{bb'}^{\mathrm{at}}(\boldsymbol{q})|^2, \tag{49}$$

where we have used (1) and (6) and Eq. (19) of [1]. We obtain the FBA to $\sigma_{\mathrm{TI}}^{B1}$ by integrating (49) over $\kappa$ and $\hat{\boldsymbol{v}}_f$ and using the Hartley-Walters approach described above to sum over all the final atomic states. If the initial Ps state $\phi_a$ is an $s$ state, then, in analogy with (35), we may define

$$G_a^{\mathrm{Ps}}(\kappa,q) \equiv \int d\hat{\boldsymbol{\kappa}}|I_{a\boldsymbol{\kappa}}^{\mathrm{Ps}}(\boldsymbol{q})|^2 \tag{50}$$

and, using $\boldsymbol{q}=2(\boldsymbol{v}_0-\boldsymbol{v}_f)$, convert the integral over $d\hat{\boldsymbol{v}}_f$ into an integral over $q$ according to

$$d\hat{\boldsymbol{v}}_f \to -\frac{\pi q dq}{2v_0 v_f}, \tag{51}$$

with the result

$$\sigma_{\mathrm{TI}}^{B1} = \frac{16\pi}{v_0^2}\sum_{nl}\int_0^{\sqrt{2\bar{E}_{nl}}} dv_T v_T^2 \int_0^{\kappa_{\max}} d\kappa\,\kappa^2 \times\int_{2|v_0-v_f|}^{2|v_0+v_f|}\frac{dq}{q^3}G_a^{\mathrm{Ps}}(\kappa,q)G_{nl}^{\mathrm{at}}(v_T,q)\frac{S(q)}{\bar{S}(q)}, \tag{52}$$

where $v_f$ is defined as a function of $\kappa$ and $v_T$ by [see (8b)]

$$v_0^2 = \kappa^2 + v_f^2 + \frac{1}{2}v_T^2 + Q_a^{\mathrm{Ps}} + Q_{nl}^{\mathrm{at}} \tag{53}$$

and

$$\kappa_{\max} = \sqrt{v_0^2 - Q_a^{\mathrm{Ps}} - Q_{nl}^{\mathrm{at}} - \frac{1}{2}v_T^2}. \tag{54}$$

### B. TT collisions

Now we consider the TT contribution, again using the FBA. Let the electron be ionized from the $nl$ shell of the target and be ejected with velocity $\boldsymbol{v}_e$ [22] into a solid angle $d\Omega_e$, and let the Ps transit from the state $\phi_a$ to $\phi_{a'}$. Then, from (1) and (32), the FBA to the corresponding DDCS is

$$\frac{d^2\sigma_{aa',nl}^{B1}}{dE_e d\Omega_e} = \frac{32v_f v_e}{v_0}\int\frac{1}{q^4}|I_{aa'}^{\mathrm{Ps}}(\boldsymbol{q})|^2|I_{nl}^{\mathrm{at}}(\boldsymbol{v}_e,\boldsymbol{q})|^2 d\hat{\boldsymbol{v}}_f, \tag{55}$$

where

$$|I_{nl}^{\mathrm{at}}(\boldsymbol{v}_e,\boldsymbol{q})|^2 \equiv \sum_m |I_{nlm}^{\mathrm{at}}(\boldsymbol{v}_e,\boldsymbol{q})|^2. \tag{56}$$

Using $\boldsymbol{q}=2(\boldsymbol{v}_0-\boldsymbol{v}_f)$ the integral over $\hat{\boldsymbol{v}}_f$ may be changed to an integral over $q$ and the azimuthal angle $\phi_q$ of $\boldsymbol{q}$ relative to $\boldsymbol{v}_0$ as $z$ axis. Then (55) becomes

$$\frac{d^2\sigma_{aa',nl}^{B1}}{dE_e d\Omega_e} = \frac{8v_e}{v_0^2}\int_0^{2\pi} d\phi_q \int_{2|v_0-v_f|}^{2|v_0+v_f|}\frac{dq}{q^3}|I_{aa'}^{\mathrm{Ps}}(\boldsymbol{q})|^2|I_{nl}^{\mathrm{at}}(\boldsymbol{v}_e,\boldsymbol{q})|^2. \tag{57}$$

The first Born cross section $d^2\sigma_{\mathrm{TT}}^{B1}/dE_e d\Omega_e$ is obtained by summing (57) over all final Ps states $\phi_{a'}$ and over all atom shells $nl$:

$$\frac{d^2\sigma_{\mathrm{TT}}^{B1}}{dE_e d\Omega_e} = \sum_{nl}\frac{d^2\sigma_{\mathrm{TT},nl}^{B1}}{dE_e d\Omega_e}, \tag{58}$$

where

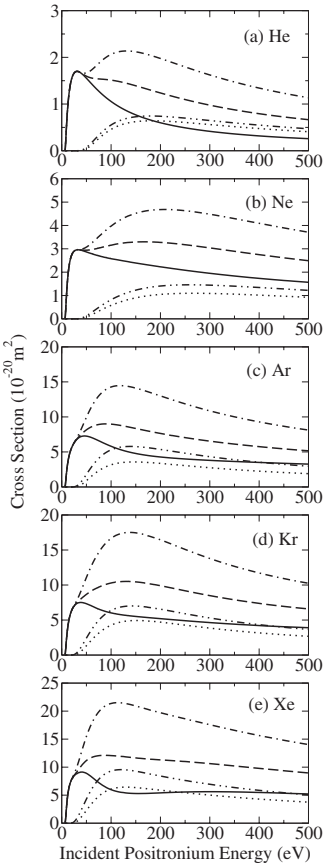


FIG. 1. Total ionization cross sections for Ps $(1s)$ collisions with ground-state (a) helium, (b) neon, (c) argon, (d) krypton, and (e) xenon. Solid curve, TE; dotted curve, TI; dash–double-dotted curve, TT; dashed curve, TOTPOS=TE+TI; dash-dotted curve, TOTELE=TE+TI+TT.

$$\frac{d^2\sigma^{B1}_{\mathrm{TT},nl}}{dE_e d\Omega_e} = \sum_{a'} \frac{d^2\sigma^{B1}_{aa',nl}}{dE_e d\Omega_e}. \tag{59}$$

Let us now assume that the initial Ps state $\phi_a$ is an $s$ state. Then, if $\phi_{a'}$ is a discrete state with quantum numbers $n_{a'}l_{a'}m_{a'}$, the sum

$$\sum_{m_{a'}} |I^{\mathrm{Ps}}_{aa'}(\boldsymbol{q})|^2 \tag{60}$$

will be a function only of $q$. The integral over $\phi_q$ in (57) then acts only upon $|I^{\mathrm{at}}_{nl}(\boldsymbol{v}_e,\boldsymbol{q})|^2$. Using (6), (50), (54), and (56), the contribution to (59) from Ps ionization may be written

$$\frac{d^2\sigma^{B1}_{a,\mathrm{ion},nl}}{dE_e d\Omega_e} = \frac{8v_e}{v_0^2}\int_0^{\kappa_{\max}} d\kappa\, \kappa^2 \int_{2|v_0-v_f|}^{2|v_0+v_f|} \frac{dq}{q^3} G^{\mathrm{Ps}}_a(\kappa,q) \times \int_0^{2\pi} d\phi_q |I^{\mathrm{at}}_{nl}(\boldsymbol{v}_e,\boldsymbol{q})|^2, \tag{61}$$

where (53) (with $\boldsymbol{v}_T$ replaced by $\boldsymbol{v}_e$) gives the functional dependence of $v_f$ on $\kappa$. From (61) we again see that the integral over $\phi_q$ acts only upon $|I^{\mathrm{at}}_{nl}(\boldsymbol{v}_e,\boldsymbol{q})|^2$. Consider therefore

$$\int_0^{2\pi} d\phi_q |I^{\mathrm{at}}_{nl}(\boldsymbol{v}_e,\boldsymbol{q})|^2. \tag{62}$$

From (39) and (56) it can be shown that

$$|I^{\mathrm{at}}_{nl}(\boldsymbol{v}_e,\boldsymbol{q})|^2 = \sum_{\lambda=0}^{\infty} \sum_{l'=|\lambda-l|}^{|\lambda+l|} \sum_{\lambda'=0}^{\infty} \sum_{l''=|\lambda'-l|}^{|\lambda'+l|} \sum_{L=|\lambda-\lambda'|}^{|\lambda+\lambda'|} A^{\star}(\lambda,l',l) \times A(\lambda',l'',l) R^{\star}(\lambda,l',l,v_e,q,n) \times R(\lambda',l'',l,v_e,q,n) \times B(\lambda,l',\lambda',l'',l,L) P_L(\hat{\boldsymbol{v}}_e\cdot\hat{\boldsymbol{q}}), \tag{63}$$

where

$$B(\lambda,l',\lambda',l'',l,L) \equiv (-1)^{\lambda'+l''-L}\frac{(2l+1)}{(4\pi)^2}[(2\lambda+1)(2l'+1) \times (2\lambda'+1)(2l''+1)]^{1/2} C(\lambda,\lambda',L,0,0,0) \times C(l',l'',L,0,0,0) W(\lambda,l,L,l'';l',\lambda'). \tag{64}$$

$\star$ denotes complex conjugation, and $W(abcd;ef)$ is the Racah coefficient as defined by Rose [18]. It is now a simple matter to integrate (63) over $\phi_q$. The result for (62) is the same as (63), but with the replacement

$$P_L(\hat{\boldsymbol{v}}_e\cdot\hat{\boldsymbol{q}}) \to 2\pi P_L(\hat{\boldsymbol{v}}_e\cdot\hat{\boldsymbol{v}}_0) P_L(\hat{\boldsymbol{q}}\cdot\hat{\boldsymbol{v}}_0). \tag{65}$$

Finally, we note that

$$\hat{\boldsymbol{q}}\cdot\hat{\boldsymbol{v}}_0 = \frac{v_0^2 - v_f^2 + q^2/4}{v_0 q}. \tag{66}$$

## IV. CALCULATIONAL DETAILS

We consider collisions of Ps $(1s)$ with the ground-state noble gases He, Ne, Ar, Kr, and Xe. All of our TE calculations have been made using the impulse approximation of [1]. The atomic orbitals $\chi_{nlm}(\boldsymbol{r})$ have been taken from [23]. The atomic ionization potentials $Q^{\mathrm{at}}_{nl}$ have been taken to be the Hartree-Fock orbital energies of [23] with the exception of that for the outermost shell where the accurate values of [24] have been used. Tabulations of the incoherent scattering function for the noble gases are available in [25–29].

In calculating the infinite sum over discrete Ps states required in (59) it is found that for large enough $n_{a'}$, where $n_{a'}$ is the principal quantum number of the state $\phi_{a'}$, the contribution of the state to the sum varies with $n_{a'}$ as (constant) $n^3_{a'}$. Consequently, the infinite sum is easily evaluated by summing up to a maximum $n_{a'}$, usually $n_{a'}=10$, and extrapolating beyond using a $1/n^3_{a'}$ scaling. The extrapolated contribution is typically small.

## V. RESULTS

### A. Total ionization cross sections

Figure 1 shows the total fragmentation cross sections $\sigma^{\mathrm{TOTPOS}}$ and $\sigma^{\mathrm{TOTELE}}$ of (15) and (20). Also exhibited are

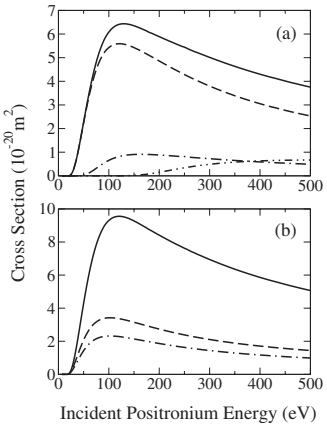


FIG. 2. TI and TT cross sections for Ps $(1s)$ colliding with Xe. (a) $\sigma_{\mathrm{TI}}^{B1}$ and the contributions to it from various shells: solid curve, $\sigma_{\mathrm{TI}}^{B1}$; dashed curve, $5p$ contribution; dash-dotted curve, $5s$ contribution; dash–double-dotted curve, $4d$ contribution. (b) $\sigma_{\mathrm{TT}}^{B1}$ and the contributions to it from discrete excitations of Ps: solid curve, $\sigma_{\mathrm{TT}}^{B1}$; dashed curve, contributions from all discrete excitations; dash-dotted curve, contribution from $\mathrm{Ps}(1s)\rightarrow\mathrm{Ps}(2p)$ excitation.

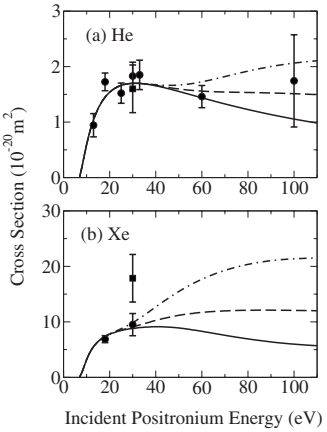


FIG. 3. Total ionization cross sections for Ps $(1s)$ collisions with ground-state (a) helium and (b) xenon. Solid curve, TE; dashed curve, TOTPOS=TE+TI; dash-dotted curve, TOTELE=TE+TI +TT. Experimental data [3,4,14,15]: solid circles, TOTPOS; solid squares, TOTELE.

their TE, TI, and TT components. The figure starkly demonstrates the need to take account of the TI and TT contributions at impact energies above about twice the ionization potential of the atom. Except for He beyond about 200 eV and Xe between 100 and 225 eV, the TI contribution is everywhere smaller than the TE cross section. The TT component, due to electrons ejected from the target, is consistently larger than the TI contribution. This effect is magnified with increasing target size as is to be expected since the larger targets have both more electrons and lower first ionization potentials.

Figure 2 highlights the contribution to $\sigma_{\mathrm{TI}}^{B1}$ coming from inner-shell excitations [see (45a) and (45b)] and the contribution of discrete Ps excitations to $\sigma_{\mathrm{TT}}^{B1}$ [see (59)]. The case shown is Xe in the impact energy range up to 500 eV. Although $\sigma_{\mathrm{TI}}^{B1}$ is dominated by excitation from the outer $5p$ shell and $\sigma_{\mathrm{TT}}^{B1}$ by Ps ionization, it is clear that we should not neglect the inner shells nor discrete excitation of the Ps, which [see Fig. 2(b)] is mostly $\mathrm{Ps}(1s)\rightarrow\mathrm{Ps}(2p)$ excitation. The same pattern is observed for the other targets, but with decreasing relative importance of inner shells and discrete Ps excitation as we move down the sequence from Xe to He [30]. At impact energies above 500 eV it is to be anticipated that the relative importance to $\sigma_{\mathrm{TT}}^{B1}$ of inner-shell excitations will increase.

Figure 3 compares our results for $\sigma^{\mathrm{TOTPOS}}$ and $\sigma^{\mathrm{TOTELE}}$ with the available experimental data [3,4,14,15]; these measurements have only been made for He and Xe targets. There is good agreement between our calculations and the measurements of $\sigma^{\mathrm{TOTPOS}}$ for both targets. Unfortunately, according to our calculations, all except one of these measurements are at energies where TI effects are unimportant and so they do not test the theory. The exceptional point, at 100 eV for the He target, is certainly in the region where target inelasticty is significant, but again unfortunately, has error bars which are too large to reveal the TI component.

There are two measurements of $\sigma^{\mathrm{TOTELE}}$, one for He and one for Xe, and both at 30 eV. According to our calculations there is little difference between $\sigma^{\mathrm{TOTPOS}}$ and $\sigma^{\mathrm{TOTELE}}$ at 30 eV, for both targets. The measurement in He is in agreement with this result, but the experimental point for Xe indicates that $\sigma^{\mathrm{TOTELE}}$ is significantly larger than $\sigma^{\mathrm{TOTPOS}}$ at 30 eV. Since [see (15) and (20)]

$$\sigma^{\mathrm{TOTELE}} = \sigma^{\mathrm{TOTPOS}} + \sigma_{\mathrm{TT}}, \tag{67}$$

this implies that we are grossly underestimating $\sigma_{\mathrm{TT}}$. It is therefore pertinent to examine our approximation to $\sigma_{\mathrm{TT}}$ more closely.

One, perhaps significant in this context, defect of the approximation $\sigma_{\mathrm{TT}}^{B1}$ is that it does not have the correct threshold. The threshold for the TT process should be at the ionization potential of the atom; in the case of Xe, this is 12.13 eV. However, because the matrix element (2a) and (2b) is zero when $\phi_a$ and $\phi_{a'}$ have the same parity, the threshold in $\sigma_{\mathrm{TT}}^{B1}$ is only reached whenever the Ps $(1s)$ projectile can be excited to Ps $(2p)$—i.e., at 12.13+5.10=17.23 eV. This delays the rise of the TT cross section, making it possibly smaller at 30 eV than it should be. Whether a better approximation could make $\sigma_{\mathrm{TT}}$ rise more quickly so that $\sigma^{\mathrm{TOTELE}}$ could pass through the error bar on the measurement at 30 eV is debatable.

Our approximation $\sigma_{\mathrm{TI}}^{B1}$ also has an incorrect threshold. In the Hartley-Walters approximation the excitation of the atom is modeled on pure ionization. Consequently, $\sigma_{\mathrm{TI}}^{B1}$ has its threshold at the ionization potential of the atom—i.e., 24.58 eV for He and 12.13 eV for Xe. However, the discrete excitations of He and Xe begin earlier at 19.81 eV and 8.32 eV, respectively. However, the agreement between experiment and our calculations of $\sigma^{\mathrm{TOTPOS}}$ for both He and Xe suggests that this failure does not have serious consequences.

### B. Single-differential cross sections

In Figs. 4 and 5 we show the SDCSs $d\sigma/dE_e$ and $d\sigma/dE_p$ for He and Xe targets at a selection of impact energies. With increasing impact energy the pattern of the cross sections for

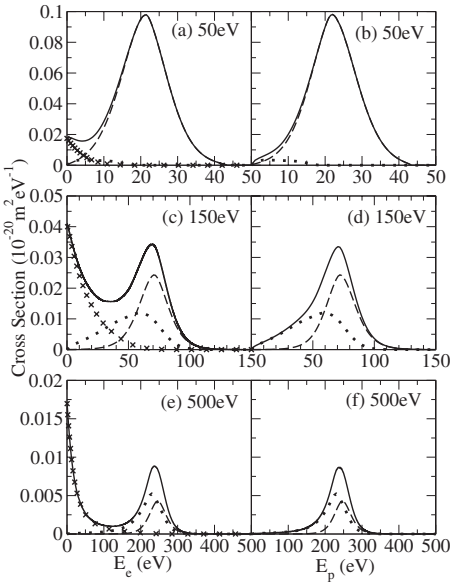


FIG. 4. Cross sections differential in ejection energy for Ps ($1s$) collisions with ground-state He at various impact energies. Solid curve, (a), (c), and (e) TOTELE=TE+TI+TT, (b), (d), and (f) TOTPOS=TE+TI; dashed curve, TE; dotted curve, TI; crosses, TT.

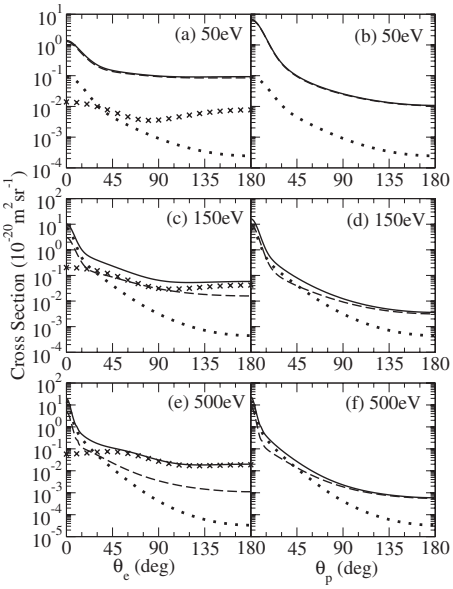


FIG. 6. Cross sections differential in ejection angle for Ps ($1s$) collisions with ground-state He at various impact energies. Solid curve, (a), (c), and (e) TOTELE=TE+TI+TT, (b), (d), and (f) TOTPOS=TE+TI; dashed curve, TE; dotted curve, TI; crosses, TT.

both targets is similar although differing in some details and in scale, the Xe cross sections being generally about a factor of 10 larger than those for He. At 50 eV the TI and TT components are almost negligible for He, but quite significant for Xe. The TE components exhibit a peak at roughly half the residual energy $E_r = v_0^2 - Q_{1s}^{\mathrm{Ps}}$. At high enough impact energy the TI components also give a peak at approximately half the maximum residual energy allowed for TI collisions in our approximation—i.e., $v_0^2 - Q_{1s}^{\mathrm{Ps}} - Q^{\mathrm{at}}$ where $Q^{\mathrm{at}}$ is the first ionization potential of the atom. The TE and TI peaks combine to form a single peak in the total cross section positioned between the two components. For $d\sigma/dE_e$ there is also a TT contribution from the ionized target electrons peaking at or near (see the case of Ar in [30]) zero ejection energy. As a result, $d\sigma^{\mathrm{TOTELE}}/dE_e$ has two peaks, one close to $\frac{1}{2}E_r$ coming from the electron ionized from the Ps, the other arising from ionized target electrons. By increasing the impact energy we can effectively separate the electrons coming from the target and the Ps.

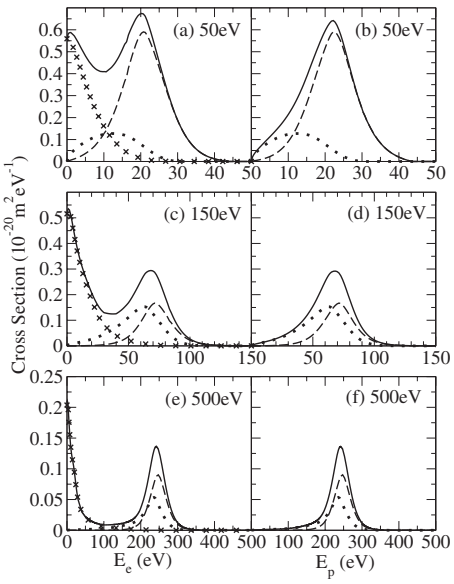


FIG. 5. Cross sections differential in ejection energy for Ps ($1s$) collisions with ground-state Xe at various impact energies. Solid curve, (a), (c), and (e) TOTELE=TE+TI+TT, (b), (d), and (f) TOTPOS=TE+TI; dashed curve, TE; dotted curve, TI; crosses, TT.

Figures 6 and 7 show $d\sigma/d\Omega_e$ and $d\sigma/d\Omega_p$ for He and Xe at a selection of impact energies. At forward angles these cross sections are dominated by TE or TI scattering, or both, depending upon the impact energy. With increasing ejection angle the TI cross section falls rapidly becoming very much smaller than the other components. This is a failing of our TI approximation. Recall that our TI cross sections are calculated in the FBA. In this approximation the interaction of the Ps with the target nucleus does not contribute to collisions in which the target is excited due to orthogonality of the initial and final states [see (2b), also (33)]. Ejection of the Ps electron or positron into large angles is very much more probable when it collides with the heavy target nucleus rather than when it collides with a light target electron. Our TI approximation is deprived of the nuclear collision, and so our large-angle TI cross sections are much too small. Nevertheless, we would still expect them to be smaller than the TE cross section, but only a better approximation than that reported here can tell us by exactly how much. For electron ejection, the TT cross section, the electron from the target, tends to dominate at large angles with increasing impact energy. We note also the structure in the TE cross section for electron ejection in Xe at the larger angles. As discussed in our previous paper [1], this reflects the structure seen in the larger-angle cross sections for elastic scattering of free electrons by Xe. Figure 7 shows that this structure is largely washed out in the full

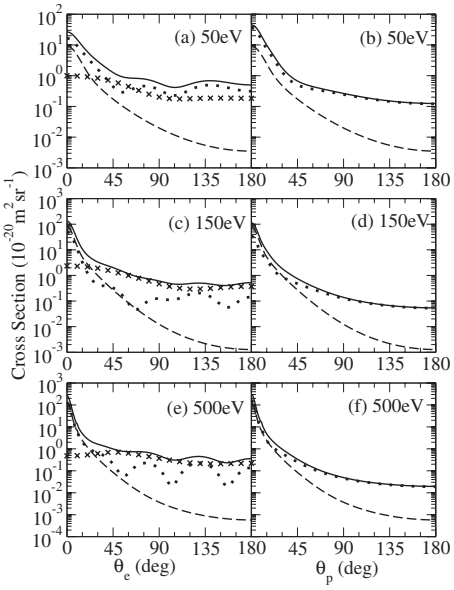


FIG. 7. Cross sections differential in ejection angle for Ps ($1s$) collisions with ground state Xe at various impact energies. Solid curve, (a), (c), and (e) TOTELE=TE+TI+TT, (b), (d), and (f) TOTPOS=TE+TI; dashed curve, TI; dotted curve, TE; crosses, TT.

cross section $d\sigma^{\mathrm{TOTELE}}/d\Omega_e$ due to masking by electrons ejected from the target. However, with a better approximation for TI scattering we would expect to see such structure emerging in the TI cross section which would make it more visible in the total $d\sigma^{\mathrm{TOTELE}}/d\Omega_e$.

Similar to Figs. 4–7, Figs. 8 and 9 show cross sections for He and Xe differential in the longitudinal energy of the

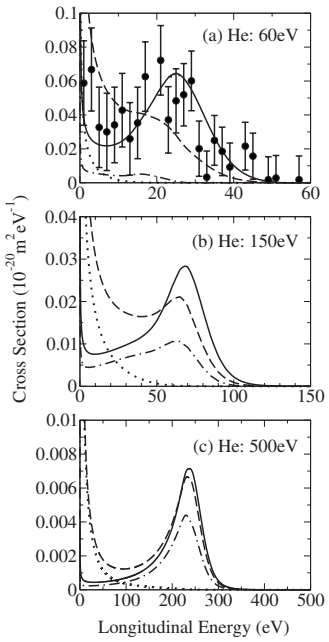


FIG. 8. Cross sections differential in longitudinal energy for Ps ($1s$) collisions with ground-state He. Solid curve, TOTPOS=TE+TI; dashed curve, TOTELE=TE+TI+TT; dash-dotted curve, TI; dotted curve, TT. Solid circles in (a) correspond to experimental measurements of TOTPOS [14].

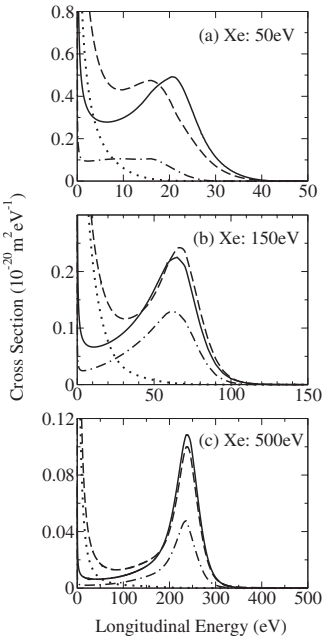


FIG. 9. Cross sections differential in longitudinal energy for Ps ($1s$) collisions with ground-state Xe. Solid curve, TOTPOS=TE+TI; dashed curve, TOTELE=TE+TI+TT; dash-dotted curve, TI; dotted curve, TT.

ejected positron and electron. The longitudinal cross section is a particular sample of the DDCS with respect to energy and angle of the ejected particle over a range of ejected energies and angles [see (46)]. Its significance stems from what is presently possible in experiment. Because of the need to have a magnetic field in the apparatus, only the energy of the liberated positron or electron in the direction of incidence can be measured. Our calculations assume that particles ejected in both the forward and backward cones are collected [see (46)]. That is the case for the positron ejection measurements that have so far been reported.

Figures 8 and 9 show a certain degree of similarity to Figs. 4 and 5 for $d\sigma/dE_e$ and $d\sigma/dE_p$, especially with increasing impact energy. However, unlike the former cross sections which go to zero for TE and TI scattering at zero ejection energy and are finite for TT scattering at zero energy, the longitudinal cross sections become infinite as $1/\sqrt{E_l}$ as the longitudinal energy $E_l \rightarrow 0$ [see (46)]. This tends to give them a more accentuated tail at low ejected energies which becomes more prominent as the impact energy is reduced. As before, there is a peak in the TE, TI, and full cross sections at roughly half the residual energy, eventually, in the case of electron ejection, leading with increasing impact energy to a, more or less, separation of electrons originating from the target and the electron ejected from the Ps.

Since our original publication on TE fragmentation [1] new measurements of the longitudinal cross section for positron ejection have been made at 60 eV [14]. These are compared with our calculations in Fig. 8(a). The measurements, which are absolute, agree well with our results, although the error bars are large (the experimental data in [14] are described as "preliminary"). Unfortunately, the measurements do not test the TI component of our cross section which, from Fig. 8(a), is seen to be small at 60 eV.

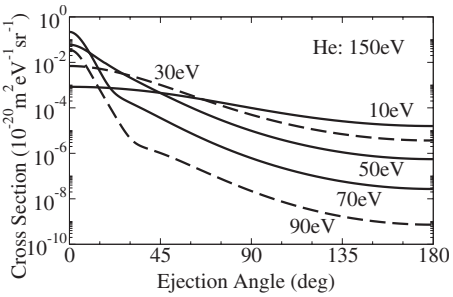


FIG. 10. TI DDCS for Ps ($1s$) collisions with ground-state He at 150 eV impact energy. Particle ejection energies label each curve.

### C. Double-differential cross sections

Measurement of the double-differential cross sections $d^2\sigma^{\mathrm{TOTELE}}/dE_e d\Omega_e$ and $d^2\sigma^{\mathrm{TOTPOS}}/dE_p d\Omega_p$ is now a real possibility [13]. In Fig. 10 we consider the TI component of both of these cross sections for a He target at an impact energy of 150 eV. In our approximation this component is the same for both cross sections [see (48a)]. At other impact energies and for other targets the general trends shown in Fig. 10 do not change. Figure 10 shows that for TI collisions the ejected electrons and positrons coming from the Ps emerge predominantly in the forward direction with approximately half the maximum residual energy $(v_0^2 - Q_{1s}^{\mathrm{Ps}} - Q^{\mathrm{at}})$. Forward ejection becomes more pronounced the higher the ejection energy. Again, we remind the reader that, because of our use of the FBA, the cross section at larger angles is unreliable, almost certainly being much too small. Nevertheless, the cross section at smaller angles should be reasonable.

In Fig. 11 we present the TT cross section $d^2\sigma_{\mathrm{TT}}^{B1}/dE_e d\Omega_e$ for a He target at impact energies of 150 eV and 500 eV; the situation is similar for the other targets. Low electron ejection energies are considered since this is where this cross section is largest, see Fig. 4. At 150 eV impact energy the TT cross section at the lowest ejection energies is peaked in the backward direction. As the ejection energy increases forward electron ejection begins to dominate. For 500 eV impact energy the situation changes somewhat. Initially, for small ejection energy, electrons are most likely to be ejected into the backward cone (90°–180°). With increasing ejection energy

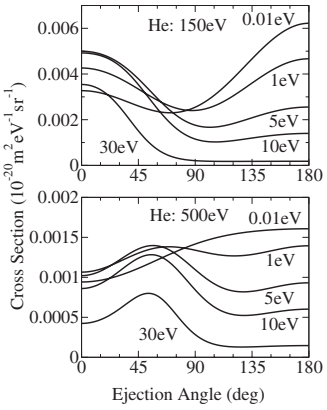


FIG. 11. $d^2\sigma_{\mathrm{TT}}^{B1}/dE_e d\Omega_e$ for Ps ($1s$) collisions with ground-state He. Electron ejection energies label each curve.

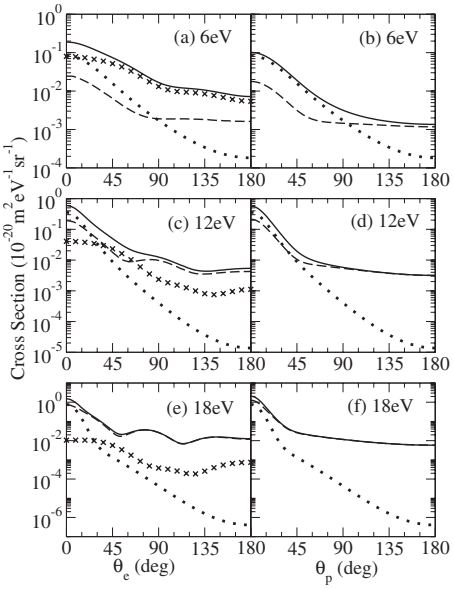


FIG. 12. $d^2\sigma/dE_e d\Omega_e$ [(a), (c), and (e)] and $d^2\sigma/dE_p d\Omega_p$ [(b), (d), and (f)] for Ps ($1s$) collisions with ground-state Xe at 50 eV. Particle ejection energy is marked on each graph. Solid curve, (a), (c), and (e) TOTELE=TE+TI+TT; (b), (d), and (f) TOTPOS =TE+TI; dashed curve, TE; dotted curve, TI; crosses, TT.

a maximum in the cross section appears in the forward cone (0°–90°).

It is of interest to see how the different components, TE, TI, and TT, contribute to the full DDCSs. This is illustrated in Fig. 12 for the case of Xe at an impact energy of 50 eV. This energy (see Fig. 3) is within the range of present experimental capability and is an energy at which the cross sections are not just dominated by TE fragmentation. We have chosen ejection energies of 6, 18, and 12 eV which, according to Figs. 5(a) and 5(b), are in regions where $d\sigma^{\mathrm{TOTELE}}/dE_e$ ($d\sigma^{\mathrm{TOTPOS}}/dE_p$) is dominated by the TT (TI), TE, and none of the components, respectively. Figures 7(a) and 7(b) show that at the same impact energy TE and TI contribute most to $d\sigma^{\mathrm{TOTELE}}/d\Omega_e$ and $d\sigma^{\mathrm{TOTPOS}}/d\Omega_p$ at small angles and TE and TT at large angles. How then does all this work out for the DDCSs?

Consider $d^2\sigma/dE_e d\Omega_e$ first, Figs. 12(a), 12(c), and 12(e). At 6 eV ejection the cross section is mostly TT except near the forward direction where TI and TT are comparable; TE is everywhere negligible. At 12 eV TI dominates at small angles, followed by TE, and TT is negligible; at large angles, TE dominates. At 18 eV the cross section is mostly TE except in the near-forward region where the TE and TI contributions are comparable. For $d^2\sigma/dE_p d\Omega_p$, Figs. 12(b), 12(d), and 12(f), TI is dominant at forward angles for 6 eV and TE at large angles. At 12 eV, TI is still dominant at small angles, but less so, and TE at large angles, but now over a larger angular range. At 18 eV TE dominates at all angles although TI is comparable near the forward direction. Figure 12 illustrates that it should be possible to more or less separate the different contributions in the DDCSs by a suitable choice of ejected energy and angular range.

This separation is again illustrated in Fig. 13 for $d^2\sigma/dE_e d\Omega_e$ for Xe at an impact energy of 500 eV. Most

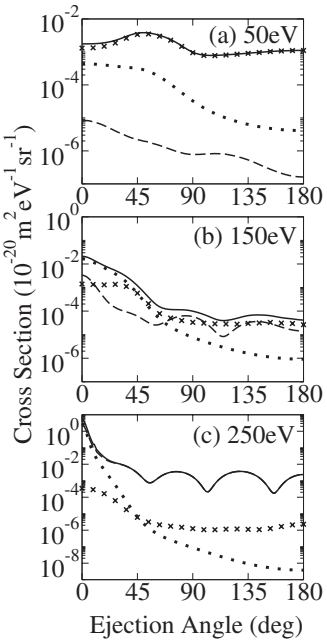


FIG. 13. $d^2\sigma/dE_e d\Omega_e$ for Ps $(1s)$ collisions with ground-state Xe at 500 eV. Electron ejection energy is marked on each graph. Solid curve, TOTELE=TE+TI+TT; dashed curve, TE; dotted curve, TI; crosses, TT.

interesting here is the clear separation of the structure in the large-angle TE cross section at an ejection energy of 250 eV. In $d\sigma/d\Omega_e$ for Xe at the same impact energy [Fig. 7(e)] we saw that this structure was masked by the TT contribution. Again, we emphasize that our TI cross section should be too small at large angles in both Figs. 12 and 13, but we do not expect that a better estimate would radically alter the general picture seen in the figures.

## VI. CONCLUSIONS

We have formulated the theory of Ps fragmentation for collisions in which the atomic target is excited or ionized. Because of the need to sum over all final atomic states, or final Ps states if ionized atomic electrons are being observed, we have elected to use the FBA. While the FBA has a number of failings, we do not consider any of them to be sufficiently severe to invalidate the generality of our results. The practicalities are that, even within the FBA, the summing over final states is a major task. The three obvious failings of the FBA are (i) that it predicts identical cross sections (48a)–(48d) for electron and positron ejection, a result which is technically only correct in the asymptotic limit; (ii) that the threshold for the TT process occurs at 5.1 eV$+Q^{\rm at}$ rather than $Q^{\rm at}$, due to the vanishing of the elastic Ps form factor (2a); (iii) that the large-angle TI cross sections for electron and positron ejection from the Ps are too small, a result of the elimination of the interaction between the Ps and the atomic nucleus in the FBA for a TI collision [see (2b)]. We do not consider (i) and (ii) to be too important. Case (iii) should only be significant when we explicitly look at large angle ejection—for example, in $d\sigma/d\Omega$ or $d^2\sigma/dE\,d\Omega$. Here we must be aware of this failing, but even if we had a better approximation to TI, we would still expect the TE and TT cross sections to dominate at large angles. In this context it is important to emphasize that the FBA to TT processes does not suffer from this large-angle failure since the ejected target electron does interact with the target nucleus through the potential $V_{nl}(r)$ of (26), the $Z$ in the form factor (2b) pertains only to the Ps-nucleus interaction. Another failing, not of the FBA itself, but of the Hartley-Walters approximation that we use to sum over atomic states, is that our threshold for TI processes is at 6.8 eV$+Q^{\rm at}$ rather than 6.8 eV$+Q^{\rm ex}$ where $Q^{\rm ex}$ is the lowest discrete excitation threshold of the atom. Again, we do not consider this to be particularly important.

Our results show clearly that excitation of the target becomes very important at impact energies greater than about 2 times the first ionization threshold of the atom. For the cross sections differential with respect to the ejected energy—e.g., $d\sigma/dE$ and $d\sigma/dE_l$—we find, except possibly at very low impact energies, that there is a peak at roughly one-half the impact energy of the Ps. This peak corresponds to electron or positron ejection from the Ps and moves with the Ps as the impact energy is changed. When ejected electrons are observed there is also a peak toward zero ejection energy coming from electrons ionized from the target atom. As a result, by increasing the impact energy we can effectively separate electrons coming from the target and the Ps. By looking at the DDCS $d^2\sigma/dE\,d\Omega$ it should also be possible to separate the TE, TI, and TT contributions by a judicious choice of ejected energy and angular range.

Presently experiment has only measured at a few impact energies, and only for He and Xe targets, the total fragmentation cross sections and the cross-section differential in the longitudinal energy of the ejected positron. Except in one case, electron ejection with a Xe target at 30 eV, there is excellent agreement between our calculations and experiment. Unfortunately, according to our theory, nearly all of the measurements are at energies where TE collisions dominate and of the two measurements which are not; the error bars are too large to test our theories of target excitation. The anomalous case of electron ejection with a Xe target at 30 eV remains a puzzle to be resolved.

Other results not shown here may be found in [30].

## ACKNOWLEDGMENTS

We are grateful to Professor G. Laricchia for providing us with data from Ref. [14]. One of us (C.S.) acknowledges support from the Department for Employment and Learning Northern Ireland.

[1] C. Starrett, M. T. McAlinden, and H. R. J. Walters, Phys. Rev. A **72**, 012508 (2005).
[2] M. T. McAlinden, F. G. R. S. MacDonald, and H. R. J. Walters, Can. J. Phys. **74**, 434 (1996).
[3] S. Armitage, D. E. Leslie, A. J. Garner, and G. Laricchia, Phys. Rev. Lett. **89**, 173402 (2002).
[4] G. Laricchia, S. Armitage, and D. E. Leslie, Nucl. Instrum. Methods Phys. Res. B **221**, 60 (2004).
[5] H. M. Hartley and H. R. J. Walters, J. Phys. B **20**, 1983 (1987).
[6] We use atomic units (a.u.) in which $\hbar=m_e=e=1$.
[7] H. R. J. Walters, J. Phys. B **6**, 1003 (1973).
[8] H. R. J. Walters, J. Phys. B **8**, L54 (1975).
[9] D. P. Dewangan and H. R. J. Walters, J. Phys. B **11**, 3983 (1978).
[10] H. M. Hartley and H. R. J. Walters, J. Phys. B **21**, L43 (1988).
[11] H. M. Hartley and H. R. J. Walters, J. Phys. B **20**, 3811 (1987).
[12] Here, in the interest of clarity, we have preferred to write $d^2\sigma^{B1}_{bb'}/dE_p d\Omega_p$ rather than $d^2\sigma^{B1}_{bb'}/dE\, d\Omega_p$ used in [1]. By conservation of energy, Eq. (8a) and (8b), $dE_p=-dE_e$, so the generic use of $dE$ is unambiguous and consistent with its use in the TDCS (4). However, at the DDCS and SDCS levels we believe that it is clearer to specifically write $dE_p$ or $dE_e$ rather than the generic $dE$.
[13] G. Laricchia (private communication).
[14] S. Armitage, D. E. Leslie, J. Beale, and G. Laricchia, Nucl. Instrum. Methods Phys. Res. B **247**, 98 (2006).
[15] S. J. Brawley, J. Beale, S. Armitage, D. E. Leslie, A. Kover, and G. Laricchia, Nucl. Instrum. Methods Phys. Res. B **266**, 497 (2008).
[16] We adopt the usual notation: $n(l)(m)$=principal (orbital) (magnetic) quantum number; $s$=spin variable; $\zeta_{s_z}$=spin function, $\zeta_{1/2}=\alpha$ (spin up), and $\zeta_{-1/2}=\beta$ (spin down).
[17] W. D. Robb, Comput. Phys. Commun. **1**, 457 (1970).
[18] M. E. Rose, *Elementary Theory of Angular Momentum* (Dover, New York, 1995).
[19] *Handbook of Mathematical Functions*, edited by M. Abramowitz and I. A. Stegun (Dover, New York, 1965).
[20] A. Nordsieck, Phys. Rev. **93**, 785 (1954).
[21] J. P. Coleman, in *Case Studies in Atomic Physics I*, edited by E. W. McDaniel and M. R. C. McDowell (North-Holland, Amsterdam, 1969), p. 101.
[22] Here we use the notation $\boldsymbol{v}_e$ rather than $\boldsymbol{v}_T$ of Sec. III A for the electron ionized from the target since now this is the electron that is being observed.
[23] E. Clementi and C. Roetti, At. Data Nucl. Data Tables **14**, 177 (1974).
[24] C. E. Moore, *Atomic Energy Levels*, Natl. Bur. Stand. (U.S.) Circ. No. 467 (U.S. GPO, Washington, D.C., 1949).
[25] C. Tavard, D. Nicholas, and M. Rouault, J. Chim. Phys. Phys.-Chim. Biol. **64**, 540 (1967).
[26] Y. K. Kim and M. Inokuti, Phys. Rev. **165**, 39 (1968).
[27] E. M. A. Peixoto, C. F. Bunge, and R. A. Bonham, Phys. Rev. **181**, 322 (1969).
[28] K. Tanaka and F. Sasak, Int. J. Quantum Chem. **5**, 157 (1971).
[29] J. H. Hubbell *et al.*, J. Phys. Chem. Ref. Data **4**, 471 (1975).
[30] C. Starrett, Ph.D. thesis, The Queen's University of Belfast, 2007.